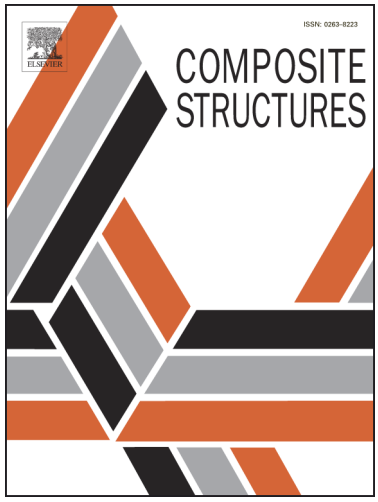

Nonlinear finite element analyses of FRP-strengthened reinforced concrete slabs using a new layered composite plate element

Xiaodan Teng, Y.X. Zhang

PII: S0263-8223(14)00143-3
DOI: http://dx.doi.org/10.1016/j.compstruct.2014.03.040
Reference: COST 5638

To appear in: *Composite Structures*

Please cite this article as: Teng, X., Zhang, Y.X., Nonlinear finite element analyses of FRP-strengthened reinforced concrete slabs using a new layered composite plate element, *Composite Structures* (2014), doi: http://dx.doi.org/10.1016/j.compstruct.2014.03.040

Nonlinear finite element analyses of FRP-strengthened reinforced concrete slabs using a new layered composite plate element

Xiaodan Teng, Y.X. Zhang*

School of Engineering and Information Technology, The University of New South Wales, Canberra, Australian Defence Force Academy, ACT 2600, Australia

**Corresponding author: Email: y.zhang@adfa.edu.au; Tel: 612-62688169*

ABSTRACT

A new layered 4-node, 24-degrees of freedom rectangular composite plate element is developed in this paper for nonlinear finite element analyses of FRP-strengthened RC slabs. The layered approach is used to form an integrated plate element for modelling of concrete, FRP, adhesive layer and steel reinforcement with a perfect bond assumption between each layer. Timoshenko's composite beam functions are employed to describe the bending behaviour of the layered plate element and shear locking problem is avoided naturally. Geometrical and material nonlinearities are both included in the new plate element. The proposed element is simple and demonstrated to be accurate and efficient for analysis of the structural behaviour of FRP-strengthened RC slabs. Once validated, the new element is also employed to investigate the effects of parameters, including the types of FRPs and strengthening scheme on the structural behaviour of FRP-strengthened RC slabs.

Keywords: Composite plate element, FRP, Nonlinear finite element analysis, Concrete slabs.

1. Introduction

Due to the great advantages of the fibre reinforced polymers (FRPs), such as a high strength-to-weight ratio, high corrosion resistance and enhanced durability, they have been used as retrofitting materials to strengthen reinforced concrete (RC) structures. A typical application of FRPs is rehabilitation of bridge components, especially bridge decks, which has become an important issue with the ageing of bridges globally. Thus, investigating the structural behaviour of FRP-strengthened concrete slabs is essential.

A number of numerical studies of the structural behaviour of FRP-strengthened concrete slabs have been reported. Reitman and Yankelevsky [1] developed a technology which was based on a nonlinear finite element (FE) grid analysis and yield-line theory for the structural analysis of FRP-strengthened concrete slabs. In the study conducted by Limam et al. [2], a three-layer FE model, in which FRP, concrete and steel were represented by a layer element was proposed. In addition a two-dimensional FE model was developed to describe elastic behaviour of CFRP-strengthened RC slabs [3].

Commercial FE software, such as ANSYS, ABAQUS and ADINA, have also been employed for nonlinear FE analyses of FRP-strengthened concrete slabs with usually different types of elements having to be used to model the concrete, steel reinforcement and FRP layers of the slabs separately which leads to complexity in establishing the FE model and excessive computational cost. For example, Tedesco et al. [4] analysed the structural behaviour of FRP-strengthened RC bridge deck using 3D 8-node solid elements for concrete, two-node truss elements for steel reinforcements and FRP laminates. Ebead and Marzouk [5] modelled the concrete using 27-node three-dimensional (3D) brick elements, the steel reinforcement using two-node truss elements and the FRP strips using eight-node thin shell elements.

In all the numerical studies mentioned above and some others [6-7], perfect bond has been assumed for simplicity of the finite element models. Although debonding between the FRP and concrete interface might be a concern [8-9], a very good bond can be achieved with the development of adhesive materials and technology.

In this paper, a layered 4-node 24-degrees of freedom (DOF) rectangular composite plate element (denoted as element CPEP) is developed for nonlinear FE analyses of FRP-strengthened concrete slabs. The element is a unified one with the concrete layers, the

smeared steel layers from the steel reinforcements, the smeared FRP layers from the FRP laminates and the adhesive layer modelled in one single element with perfect bond between the FRP, concrete and reinforcement assumed. The in-plane displacement functions of a quadrilateral plane element with drilling DOFs as used by Zhang et al. [10] are employed for the in-plane displacement of the element CPEP. Both geometric and material nonlinearities, which incorporate tension, compression, concrete cracking and tension stiffening, are included in this element. Perfect bond between the FRP, concrete and reinforcement is assumed. The nonlinear structural behaviour of FRP-strengthened concrete slabs with different types and width of FRPs, and various spacing between FRPs is investigated in the parametric studies using the developed element after validation

Timoshenko's beam function method has been proven to be simple and efficient for alleviating the shear-locking effect in FE analyses of plates and beams when used to construct plate and beam elements. The Timoshenko's composite beam functions were developed and employed to construct two simple and efficient displacement-based quadrilateral elements for linear and geometric nonlinear analysis of composite laminated plates by Zhang and Kim [11-12]. They were then extended and employed for developing of a layered shear-flexural plate/shell element for nonlinear analysis of reinforced concrete plates by Zhang et al. [10], which were then further developed for nonlinear analysis of moderately thick reinforced concrete slabs at elevated temperatures [13]. Furthermore, Zhang and Zhu [14] developed a new shear-flexible FRP-reinforced concrete slab element for nonlinear finite element analysis of FRP reinforced concrete slabs. Also, the Timoshenko's composite beam functions have been further extended and used to construct a series of composite beam elements for analysis of composite beams by Lin and Zhang [15] and steel/FRP reinforced concrete beams without and with bond-slip by Zhang and Lin [16] and Lin and Zhang [17]. In this paper, the Timoshenko's composite beam functions are extended and used for developing a composite

layered plate element for nonlinear FE analysis of FRP strengthened RC slabs. Shear deformation effects are included in the element and shear locking is avoided naturally by using the Timoshenko's composite beam functions.

2. A New Layered Composite Plate Element and Basic Formulations

The proposed 4-node 24-DOF layered rectangular plate element CPEP is shown in Fig. 1. There are six engineering DOFs per node for the proposed element, i.e., the translational displacement components u, v, w, the rotational components around the x and y axes θ_x, θ_y and the rotational (drilling) DOF θ_z. The cross-section of the element consists of concrete layers, steel layers of the smeared steel reinforcement, FRP layer of the smeared FRP and adhesive layer as shown in Fig. 1(a). The smeared steel layer is of equivalent thickness $t_s = A_s / b$, where A_s represents the area of single steel bar and b is space between two bars. The equivalent thickness of the smear FRP layer is determined by $t_{FRP} = A_{FRP} \times \mathrm{t}_0 / A_{slab}$, where A_{FRP} and A_{slab} represents the total area of the bonded FRP plates and strengthening slab respectively, and t_0 is the physical thickness of a single FRP plate.

It is assumed that each layer is in a state of plane stress, that compatibility exists and perfect bond is assumed between the steel, FRP and concrete layers. For each layer, the stress points are taken as the Gaussian points at its mid-surface. Based on the Mindlin-Reissner plate theory, the displacement component u, v, w in the direction at a point (x, y, z) in a plate element can be expressed by the corresponding mid-plane translational displacement components u^0, v^0, w^0 and rotations of the mid-plane normal around x and y axes θ_x, θ_y as

$$\begin{cases} u(x, y, z) = u^0(x, y) + z\theta_x(x, y) \\ v(x, y, z) = v^0(x, y) + z\theta_y(x, y) \\ w(x, y) = w^0(x, y) \end{cases} \tag{1}$$

The strain vector at any point in the plate element can be written as

$$\varepsilon = \varepsilon_m + \varepsilon_b \tag{2}$$

where the bending strain is expressed as

$$\varepsilon_b = \left\langle \frac{\partial \theta_x}{\partial x} \quad \frac{\partial \theta_y}{\partial y} \quad \left(\frac{\partial \theta_x}{\partial y} + \frac{\partial \theta_y}{\partial x} \right) \right\rangle^T = [B_b]\{q_b^e\} \tag{3}$$

and the membrane strain is

$$\varepsilon_m = \varepsilon_m^l + \varepsilon_m^{nl} \tag{4}$$

in which the linear and nonlinear membrane strains are

$$\varepsilon_m^l = \left\langle \frac{\partial u^0}{\partial x} \quad \frac{\partial v^0}{\partial y} \quad \frac{\partial u^0}{\partial y} + \frac{\partial v^0}{\partial x} \right\rangle^T = [B_m]\{q_m^e\} \tag{5}$$

$$\varepsilon_m^{nl} = \left\langle \frac{1}{2}\left(\frac{\partial w}{\partial x} \right)^2 \quad \frac{1}{2}\left(\frac{\partial w}{\partial y} \right)^2 \quad \frac{\partial w}{\partial x}\frac{\partial w}{\partial y} \right\rangle^T \tag{6}$$

In addition, the transverse shear strain vector is defined as

$$\gamma = \langle \gamma_{xz} \quad \gamma_{yz} \rangle = \left\langle \theta_x - \frac{\partial w}{\partial x} \quad \theta_y - \frac{\partial w}{\partial y} \right\rangle^T = [B_s]\{q_b^e\} \tag{7}$$

where $\{q_m^e\}$ and $\{q_b^e\}$ are the element nodal in-plane displacement vector and nodal bending displacement vectors, and they are expressed as

$$\{q_m^e\} = \{q_m^1 \quad q_m^2 \quad q_m^3 \quad q_m^4\} \text{ in which } \{q_m^i\} = \{u_i \quad v_i \quad \theta_{zi}\}^T \tag{8-a}$$

$$\{q_b^e\} = \{q_b^1 \quad q_b^2 \quad q_b^3 \quad q_b^4\} \text{ in which } \{q_b^i\} = \{w_i \quad \theta_{xi} \quad \theta_{yi}\}^T \tag{8-b}$$

2.1 Timoshenko's composite beam functions

The Timoshenko's composite beam functions used to represent the bending displacement of the composite plate element for FE analysis of RC slabs [10] are modified, and employed for the analysis of FRP-strengthened RC slabs in this paper. The Timoshenko's composite beam functions which satisfy the boundary condition for the displacement w and rotation θ at two ends of an beam element of length L, width b and thickness t, are given as

$$w = \left[L_1 + \mu_e L_1 L_2 (\mathrm{L}_1 - \mathrm{L}_2)\right] w_1 + \left[L_1 L_2 + \mu_e L_1 L_2 (\mathrm{L}_1 - \mathrm{L}_2)\right] \frac{L}{2} \theta_1 + \left[L_2 + \mu_e L_1 L_2 (\mathrm{L}_2 - \mathrm{L}_1)\right] w_2 + \left[-L_1 L_2 + \mu_e L_1 L_2 (\mathrm{L}_1 - \mathrm{L}_2)\right] \frac{L}{2} \theta_2 \tag{9-a}$$

$$\theta = -\left(\frac{6 L_1 L_2}{L \mu_e}\right) w_1 + \left[L_1 \left(1 - 3\mu_e L_2\right)\right] \theta_1 + \left(\frac{6 L_1 L_2}{L \mu_e}\right) w_2 + \left[L_2 \left(1 - 3\mu_e L_1\right)\right] \theta_2 \tag{9-b}$$

in which

$$L_1 = 1 - \frac{x}{L}; \quad L_2 = \frac{x}{L}; \quad \mu_e = \frac{1}{1 + 12\lambda_e}; \quad \lambda_e = \frac{\bar{Q}_b}{\bar{Q}_s L^2} \tag{10}$$

and $\bar{Q}_b, \bar{Q}_s$ are the bending and shear constant, respectively.

For an element side ij of the rectangular plate element with two nodes i and j, the interpolation of the normal $\tilde{\theta}_n$ and tangential $\tilde{\theta}_s$ slopes are expressed as

$$\tilde{\theta}_n = L_i \theta_{ni} + L_j \theta_{nj} \tag{11}$$

$$\tilde{\theta}_s = -\left(6 L_i L_j \big/ S_{ij}\right) \mu_{ij} w_i + L_i \left(1 - 3\mu_{ij} L_j\right) \theta_{si} + \left(6 L_i L_j \big/ S_{ij}\right) \mu_{ij} w_j + L_j \left(1 - 3\mu_{ij} L_i\right) \theta_{sj} \tag{12}$$

where θ_{ni}, θ_{si} and θ_{nj}, θ_{sj} are the normal and tangential slopes at nodes i and j, respectively, in which

$$L_1 = 1 - \frac{x}{S_{ij}}; \quad L_2 = \frac{x}{S_{ij}}; \quad \mu_e = \frac{1}{1 + 12\lambda_{ij}}; \quad \lambda_e = \frac{\bar{Q}_{bij}}{\bar{Q}_{sij} S_{ij}^2} \tag{13}$$

where x is the coordinate along the element side, S_{ij} is the length of its side ij, and $\bar{Q}_{bij}, \bar{Q}_{sij}$ is the bending and shear elastic constant of side ij respectively. For a thin plate ($t \to 0$) with a side length S_{ij}, $t / S_{ij} \to 0$ and then $\lambda_{ij} \to 0$ since $\bar{Q}_{bij} / \bar{Q}_{sij}$ is a function of t^2 and so $\mu_{ij} \to 1$. Therefore, the displacement $\tilde{\theta}_s$ on the side is the familiar rotational displacement of a thin plate. It can be clearly seen that the shear locking problem is alleviated and unified representation of the displacement functions are derived for both thick and thin plates by employing the Timoshenko's beam composite functions.

In the developed element CPEP, considering the contributions of the concrete, steel, FRP and adhesive layers, the bending and shear elastic constants are

$$\bar{Q}_{bij} = \frac{1}{3}\sum_{i=1}^{n_c} (\bar{Q}_{11}^i)_{cij} (z_{i+1}^3 - z_i^3) + \sum_{j=1}^{n_s} (\bar{Q}_{11}^j)_{sij} z_j^2 t_{s,j} + (\bar{Q}_{11})_{FRPij} z_{FRP}^2 t_{FRP} + (\bar{Q}_{11})_{aij} z_a^2 t_a \qquad (14\text{-a})$$

$$\bar{Q}_{sij} = \sum_{i=1}^{n_c} (\bar{Q}_{55}^i)_{cij} (z_{i+1} - z_{i+1}) + \sum_{j=1}^{n_s} (\bar{Q}_{55}^j)_{sij} t_{s,j} + (\bar{Q}_{55})_{FRPij} t_{FRP} + (\bar{Q}_{55})_{aij} t_a \qquad (14\text{-b})$$

in which

$$\left(\bar{Q}_{11}^i\right)_{cij} = Q_{11c}^i (\cos^4\theta_{ij} + \sin^4\theta_{ij}) + 2(Q_{12c}^i + Q_{66c}^i)\cos^2\theta_{ij}\sin^2\theta_{ij} \qquad (15\text{-a})$$

$$\left(\bar{Q}_{11}^j\right)_{sij} = Q_{11s}^j (\cos^4\theta_{ij} + \sin^4\theta_{ij}) + 2(Q_{12s}^j + Q_{66s}^j)\cos^2\theta_{ij}\sin^2\theta_{ij} \qquad (15\text{-b})$$

$$\left(\bar{Q}_{11}\right)_{FRPij} = Q_{11FRP} (\cos^4\theta_{ij} + \sin^4\theta_{ij}) + 2(Q_{12FRP} + Q_{66FRP})\cos^2\theta_{ij}\sin^2\theta_{ij} \qquad (15\text{-c})$$

$$\left(\bar{Q}_{11}\right)_{aij} = Q_{11a} (\cos^4\theta_{ij} + \sin^4\theta_{ij}) + 2(Q_{12a} + Q_{66a})\cos^2\theta_{ij}\sin^2\theta_{ij} \qquad (15\text{-d})$$

$$\left(\bar{Q}_{55}\right)_{cij} = \frac{E_c}{2(1+\nu_c)}; \quad \left(\bar{Q}_{55}\right)_{sij} = \frac{E_s}{2(1+\nu_s)}; \quad \left(\bar{Q}_{55}\right)_{FRPij} = \frac{E_{FRP}}{2(1+\nu_{FRP})}; \quad \left(\bar{Q}_{55}\right)_{aij} = \frac{E_a}{2(1+\nu_a)} \qquad (15\text{-e})$$

where Q_{11c}^i, Q_{12c}^i and Q_{66c}^i are the elastic constants of the i^{th} layer of concrete, Q_{11s}^j, Q_{12s}^j and Q_{66s}^j are the elastic constants of the j^{th} layer of steel and Q_{11FRP}, Q_{12FRP} and Q_{66FRP} are the

elastic constants of FRP layer, and Q_{11a}, Q_{12a} and Q_{66a} are the elastic constants of the adhesive layer. They are given as

$$Q^i_{11c} = \frac{E_c}{1-\nu_c^2}; \quad Q^i_{12c} = \frac{\nu_c E_c}{1-\nu_c^2}; \quad Q^i_{66c} = \frac{E_c}{2(1+\nu_c)} \tag{16-a}$$

$$Q^j_{11s} = \frac{E_s}{1-\nu_s^2}; \quad Q^j_{12s} = \frac{\nu_s E_s}{1-\nu_s^2}; \quad Q^j_{66s} = \frac{E_s}{2(1+\nu_s)} \tag{16-b}$$

$$Q_{11FRP} = \frac{E_{FRP}}{1-\nu_{FRP}^2}; \quad Q_{12s} = \frac{\nu_{FRP} E_{FRP}}{1-\nu_{FRP}^2}; \quad Q_{66FRP} = \frac{E_{FRP}}{2(1+\nu_{FRP})} \tag{16-c}$$

$$Q_{11a} = \frac{E_a}{1-\nu_a^2}; \quad Q_{12a} = \frac{\nu_a E_a}{1-\nu_a^2}; \quad Q_{66a} = \frac{E_a}{2(1+\nu_a)} \tag{16-d}$$

where E_c, E_s, E_{FRP}, E_a are the Young's modulus, and $\nu_c, \nu_s, \nu_{FRP}, \nu_a$ are the Poisson's ratio of the concrete, steel reinforcement, FRP and adhesive, respectively, and θ_{ij} is the angle between the global x axis and element side ij of the layer.

2.2 Bending strain

The bending displacement and rotation of a side of the proposed element are deduced from the Timoshenko's beam composite functions presented above using the similar method as that in Zhang et al.'s paper [10] for the analysis of RC slabs. The rotational components θ_x and θ_y around the x and y axes are expressed as

$$\langle \theta_x \quad \theta_x \rangle = \left[\bar{N}\right] \{q_b^e\} \tag{17}$$

where more details of $\left[\bar{N}\right]$ can be found in Zhang et al's paper (2007).

Then, the bending strain vector is given as

$$\varepsilon_b = \left\langle \frac{\partial \theta_x}{\partial x} \quad \frac{\partial \theta_y}{\partial y} \quad \left(\frac{\partial \theta_x}{\partial y} + \frac{\partial \theta_y}{\partial x} \right) \right\rangle^T = [B_b] \{q_b^e\} \tag{18}$$

where $[B_b]=[B_{b1} \quad B_{b2} \quad B_{b3} \quad B_{b4}]$ and $[B_{bi}]$ can be found in the Zhang et al.'s paper [10].

2.3 Membrane strain

Similar to the finite element for the analysis of RC slabs [10], the membrane displacement function of a quadrilateral element with drilling DOFs [18] is used to represent the in-plane displacements of the proposed model, with the membrane strain vector given as

$$\varepsilon_m = \left\langle \frac{\partial u^0}{\partial x} \quad \frac{\partial v^0}{\partial y} \quad \left(\frac{\partial u^0}{\partial y} + \frac{\partial v^0}{\partial x} \right) \right\rangle^T = [B_m]\{q_m^e\} \tag{19}$$

where $[B_m]=[B_{m1} \quad B_{m2} \quad B_{m3} \quad B_{m4}]$ with $[B_{mi}]$ (i=1, 2, 3, 4), and the $[B_{mi}]$ is similar to that in Zhang et al's paper [10].

2.4 Transverse shear strain

The vector of the transverse shear strains of the new element can be expressed in terms of natural coordinates as

$$\gamma = \langle \gamma_{xz} \quad \gamma_{yz} \rangle^T = [B_s]\{q_b^e\} \tag{20}$$

The transverse shear strain matrix $[B_s]$ is of the same expression as that in Zhang et al's paper [10].

3. General Constitutive Relationship

Assuming that the material properties of each layer are constant throughout its thickness, the material property matrices of the element are obtained by algebraically summing the contributions of each layer as given in Eq. (22-a) to (22-d).

$$D = \begin{bmatrix} D_{mm} & D_{mb} & 0 \\ & D_{bb} & 0 \\ sym & & D_{ss} \end{bmatrix} \tag{21}$$

where D_{mm} is the extensional stiffness, D_{bb} is the bending stiffness, D_{mb} is the bending-extensional coupling stiffness and D_{ss} is the transverse stiffness given as

$$D_{mm} = \sum_{i=1}^{n_c} D_{c,i}(z_{i+1} - z_i) + \sum_{j=1}^{n_s} D_{s,j} t_{s,j} + D_{FRP} t_{FRP} + D_a t_a \quad (22\text{-a})$$

$$D_{bb} = \sum_{i=1}^{n_c} D_{c,i}(z_{i+1}^3 - z_i^3) + \sum_{j=1}^{n_s} D_{s,j} z_j^2 t_{s,j} + D_{FRP} t_{FRP} z_{FRP}^2 + D_a t_a z_a^2 \quad (22\text{-b})$$

$$D_{mb} = \sum_{i=1}^{n_c} D_{c,i}(z_{i+1}^2 - z_i^2) + \sum_{j=1}^{n_s} D_{s,j} z_j t_{s,j} + D_{FRP} t_{FRP} z_{FRP} + D_a t_a z_a \quad (22\text{-c})$$

$$D_{ss} = k \sum_{i=1}^{n_c} D_{co,i}(z_{i+1} - z_i) \quad (22\text{-d})$$

where n_c and n_s is the number of concrete layers and smeared steel layers respectively, $D_{c,i}$ $D_{s,j}$, D_{FRP} and D_a are the in-plane material property matrices of the i^{th} concrete layer, j^{th} steel layer, FRP layer and adhesive layer respectively, $D_{co,i}$ is the out-of-plane material property matrix of the i^{th} concrete layer, z_{i+1} and z_i is the coordinate of the upper and lower surfaces of the i^{th} concrete layer in the z direction respectively, z_j is the coordinate of the mid-height of the j^{th} steel layer in the z direction, z_{FRP} is the coordinate of the mid-height of the FRP layer in the z direction, z_a is the coordinate of the mid-height of the adhesive layer in the z direction, t_s is the thickness of the j^{th} steel layer, t_{FRP} is the thickness of the FRP layer, and t_a is the thickness of the adhesive layer. k is a constant representing the non-uniformity of the shearing stress, which is generally set to be $5/6$ [19].

4. Material Models

4.1 Material model of steel, FRP and adhesive layer

The reinforcing steel is assumed to be elastic–perfectly plastic in tension and compression, with axial stiffness in only the bar direction, as shown in Fig. 2. FRPs are assumed to be linear elastic until the tension stress reaches its ultimate strength which causes brittle rupture and then reduces to zero as shown in Fig. 3. The adhesive layer is considered to be elastic-perfectly plastic in tension [20], and the in-plane material property matrix D_a in Eq. (22) is given by Eq. (23).

$$D_a = \frac{E_a}{1-\nu_a^{\,2}} \begin{bmatrix} 1 & \nu_a & 0 \\ \nu_a & 1 & 0 \\ 0 & 0 & \dfrac{1-\nu_a}{2} \end{bmatrix} \tag{23}$$

where E_a and ν_a is the elastic modulus and Poisson's ratio of adhesive layer respectively.

4.2 Material model of concrete

Before cracking or crushing, the concrete is assumed to be isotropic and linear elastic. The in-plane and out-out-plane material stiffness matrices $[D_{ci}], [D_{co}]$ are given by

$$[D_{ci}] = \frac{E_c}{1-\nu_c^2} \begin{bmatrix} 1 & \nu_c & 0 \\ \nu_c & 1 & 0 \\ 0 & 0 & \dfrac{1-\nu_c}{2} \end{bmatrix}; \quad [D_{co}] = \frac{E_c}{2(1+\nu_c)} \begin{bmatrix} 1 & 0 \\ 0 & 1 \end{bmatrix} \tag{24}$$

For concrete in compression, more complex constitutive relationship, e.g. nonlinear elastic, hypoelastic and plastic with isotropic hardening or kinematic hardening, are available. However, computational time with these constitutive relationships is excessively increased with little improvement in accuracy [10, 21]. Thus, the concrete is assumed to be elastic-perfectly plastic to simplify the model, in which a limiting compressive strain $\varepsilon_{cu} = 0.0035$ is

assumed. Once the compressive strain reaches to the limit, the concrete is assumed to crush and possess no strength.

For concrete in tension, the maximum principal stress criterion is used to identify cracking. When the maximum principal stress at the Gaussian points reaches the concrete tensile strength, cracks are assumed to form in planes perpendicular to the direction of the maximum principal tensile stress, with the elastic modulus and Poisson's ratio are reduced to zero in the maximum principal stress direction. '1' and '2' represents the directions of maximum and minimum principal stress respectively. Once the maximum principal stress in direction 1 reaches the concrete tensile strength f_t, the in-plane material property matrix $\left[D_{ci}^{'}\right]$ in the principal coordinate system is expressed as

$$\left[D_{ci}^{'}\right]=diag\left[0 \quad E_c \quad G_{12}^{c}\right] \tag{25-a}$$

When the minimum principal stress in direction 2 also reaches f_t, a second crack plane perpendicular to the first one is assumed to form, and then the in-plane property matrix $\left[D_{ci}^{'}\right]$ becomes

$$\left[D_{ci}^{'}\right]=diag\left[0 \quad 0 \quad \frac{1}{2}G_{12}^{c}\right] \tag{25-b}$$

where the G_{12}^{c} represents the cracked shear modulus that accounts for aggregate interlocking and dowel action in the smeared cracking model, and is from Cedolin and Deipoli's paper [22]. After cracking, the out-of-plane material property matrix in the principal coordinate system becomes

$$\left[D_{co}^{'}\right]=diag\left[G_{13}^{c} \quad G_{23}^{c}\right] \tag{26}$$

where the cracked shear moduli G_{13}^{c} and G_{23}^{c} suggested by Cedolin and Deipoli [22] are utilized in this study, which account for aggregate interlock and dowel action. After cracking, tension-stiffening effects become significant and must be included in the analysis. The material model for concrete in tension proposed by Izumo et al. [23] (shown in Fig. 4) is adopted herein, in which tension-stiffening effect has been taken into account. It should be noted that the material models for the steel reinforcement and concrete have been adopted in the element developed by Zhang et al. [10] for FE analysis of RC slabs.

5. Nonlinear finite element formulations

5.1 General formulation

The total Lagrangian approach, which takes the original configuration as the reference, is used for the nonlinear FE analysis of the FRP-strengthened RC slabs which is formulated as

$$\left(\left[K\right]+\left[K_{\sigma}\right]\right)\left\{\Delta q\right\}=\left\{P^{t+\Delta t}\right\}-\left\{R^{t}\right\} \tag{27-a}$$

where

$$\left[K\right]=\sum_{e}\left[K_{e}\right];\quad \left[K_{\sigma}\right]=\sum_{e}\left[K_{\sigma}^{e}\right];\quad R^{t}=\sum_{e}R_{e}^{t} \tag{27-b}$$

The element stiffness matrix $\left[K_{e}\right]$, geometric stiffness matrix $\left[K_{\sigma}^{e}\right]$ and internal force vector $\left\{R_{e}^{t}\right\}$ and the external load vector $\left\{P^{t+\Delta t}\right\}$ are defined in the following sub-sections.

5.2 Element stiffness matrix

Eq. (28) is used to calculate the element stiffness matrix $\left[K_{e}\right]$ in which A_{e} represents the area of element and $\left[D\right]$ is the material property matrix of the element given by Eq. (21).

$$\left[K_{e}\right]=\int_{A_{e}}\left[B\right]^{T}\left[D\right]\left[B\right]dA_{e} \tag{28}$$

For geometrically nonlinear analysis, strain matrix $[B]$ is written as the sum of its linear and nonlinear components as

$$[B]=\left[B^{l}\right]+\left[B^{nl}\right] \tag{29}$$

where $\left[B^{l}\right]$ is the linear strain matrix and $\left[B^{nl}\right]$ is the nonlinear strain matrix. $\left[B^{l}\right]$ is given in Eq. (30-a) which contains linear membrane strain matrix $[B_{mi}]$, bending strain matrix $[B_{bi}]$ and transverse shear strain matrix $[B_{si}]$.

$$\left[B^{l}\right]=\left[B_1^{l},B_2^{l},B_3^{l},B_4^{l}\right] \text{ with } \left[B_i^{l}\right]=\begin{bmatrix} B_{mi} & 0 \\ 0 & B_{bi} \\ 0 & B_{si} \end{bmatrix} \quad (i=1,2,3,4) \tag{30-a}$$

$$\left[B^{nl}\right]=\left[B_1^{nl},B_2^{nl},B_3^{nl},B_4^{nl}\right] \text{ with } \left[B_i^{nl}\right]=\begin{bmatrix} 0 & B_{mi}^{nl} \\ 0 & 0 \\ 0 & 0 \end{bmatrix} \quad (i=1,2,3,4) \tag{30-b}$$

The nonlinear strain matrix $\left[B^{nl}\right]$ consists of the nonlinear membrane strain matrix $\left[B_{mi}^{nl}\right]$ where the expression of $\left[B_{mi}^{nl}\right]$ is similar to that in Zhang et al's paper (2007).

5.3 Element geometric stiffness matrix

The element geometric stiffness matrix $\left[K_{\sigma}^{e}\right]$ is obtained from the following equations.

$$K_{\sigma}^{e}dq=\int_{A_e} dB^{T}\sigma_{L}dA_{e} \tag{31}$$

In component form, the element geometric stiffness matrix can be written as

$$\left[K_{\sigma_{ij}}^{e}\right]=\begin{bmatrix} 0 & 0 \\ 0 & K_{m\sigma_{ij}} \end{bmatrix} \text{ with } K_{m\sigma_{ij}}=\int_{A_e}\left[G_i\right]^{T}\left[\sigma_{L}\right]\left[G_j\right]dA_{e} \tag{32}$$

in which

$$[\sigma_L]=\begin{bmatrix} N_x & N_{xy} \\ N_{yx} & N_y \end{bmatrix} \tag{33}$$

Where N_x, N_y, N_{xy} are the membrane forces in the element mid-surface given by Eqs. (35-a) to (35-c).

5.4 Element internal force vector

The element internal force is given by

$$\{R_e^t\}=\int_{A_e}[B]^T[\sigma]dA_e \tag{34}$$

in which $[\sigma]=[N \quad M \quad T]^T$ is the general form of stress, $[N]=[N_x \quad N_y \quad N_{xy}]^T$ is membrane force vector defined at the mid-plane, $[M]=[M_x \quad M_y \quad M_{xy}]^T$ is the bending moment vector and $[T]=[Q_x \quad Q_y]^T$ is the transverse shear force vector.

$$N_x=\sum_{i=1}^{n_c}\sigma_x^i(z_{i+1}-z_i)+\sum_{j=1}^{n_s}\sigma_x^j t_s+\sigma_x^F t_{FRP}+\sigma_x^a t_a \tag{35-a}$$

$$N_y=\sum_{i=1}^{n_c}\sigma_y^i(z_{i+1}-z_i)+\sum_{j=1}^{n_s}\sigma_y^j t_s+\sigma_y^F t_{FRP}+\sigma_y^a t_a \tag{35-b}$$

$$N_{xy}=\sum_{i=1}^{n_c}\sigma_{xy}^i(z_{i+1}-z_i)+\sum_{j=1}^{n_s}\sigma_{xy}^j t_s+\sigma_{xy}^F t_{FRP}+\sigma_{xy}^a t_a \tag{35-c}$$

$$M_x=\sum_{i=1}^{n_c}z_i\sigma_x^i(z_{i+1}-z_i)+\sum_{j=1}^{n_s}z_j\sigma_x^j t_s+z_{FRP}\sigma_x^F t_{FRP}+z_a\sigma_x^a t_a \tag{35-d}$$

$$M_y=\sum_{i=1}^{n_c}z_i\sigma_y^i(z_{i+1}-z_i)+\sum_{j=1}^{n_s}z_j\sigma_y^j t_s+z_{FRP}\sigma_y^F t_{FRP}+z_a\sigma_y^a t_a \tag{35-e}$$

$$M_{xy}=\sum_{i=1}^{n_c}z_i\sigma_{xy}^i(z_{i+1}-z_i)+\sum_{j=1}^{n_s}z_j\sigma_{xy}^j t_s+z_{FRP}\sigma_{xy}^F t_{FRP}+z_a\sigma_{xy}^a t_a \tag{35-f}$$

$$Q_x=\sum_{i=1}^{n_c}\tau_{xz}^i(z_{i+1}-z_i);\quad Q_y=\sum_{i=1}^{n_c}\tau_{yz}^i(z_{i+1}-z_i) \tag{35-g}$$

The respective stress increments $\Delta\sigma$ in the concrete, steel, FRP and adhesive layers in the next $(n+1)^{th}$ iteration for the updated stress vector σ are

$$\left(\sigma^{i}\right)^{n+1} = \left(\sigma^{i}\right)^{n} + \Delta\sigma^{i} \tag{36-a}$$

$$\left(\sigma^{j}\right)^{n+1} = \left(\sigma^{j}\right)^{n} + \Delta\sigma^{j} \tag{36-b}$$

$$\left(\sigma^{F}\right)^{n+1} = \left(\sigma^{F}\right)^{n} + \Delta\sigma^{F} \tag{36-c}$$

$$\left(\sigma^{a}\right)^{n+1} = \left(\sigma^{a}\right)^{n} + \Delta\sigma^{a} \tag{36-d}$$

where

$$\Delta\sigma^{i} = \left[D_{c,i}\right]\left(\left[B_{m}\right]\left\{\Delta q_{m}^{e}\right\} + z\left[B_{b}\right]\left\{\Delta q_{b}^{e}\right\} + \left[B_{m}^{nl}\right]\left\{\Delta q_{b}^{e}\right\}\right) \tag{37-a}$$

$$\Delta\sigma^{j} = \left[D_{\mathrm{s,j}}\right]\left(\left[B_{m}\right]\left\{\Delta q_{m}^{e}\right\} + z\left[B_{b}\right]\left\{\Delta q_{b}^{e}\right\} + \left[B_{m}^{nl}\right]\left\{\Delta q_{b}^{e}\right\}\right) \tag{37-b}$$

$$\Delta\sigma^{F} = \left[D_{FRP}\right]\left(\left[B_{m}\right]\left\{\Delta q_{m}^{e}\right\} + z\left[B_{b}\right]\left\{\Delta q_{b}^{e}\right\} + \left[B_{m}^{nl}\right]\left\{\Delta q_{b}^{e}\right\}\right) \tag{37-c}$$

$$\Delta\sigma^{a} = \left[D_{a}\right]\left(\left[B_{m}\right]\left\{\Delta q_{m}^{e}\right\} + z\left[B_{b}\right]\left\{\Delta q_{b}^{e}\right\} + \left[B_{m}^{nl}\right]\left\{\Delta q_{b}^{e}\right\}\right) \tag{37-d}$$

where $\Delta\sigma^{i}$ is the stress increment in the i^{th} concrete layer, $\Delta\sigma^{j}$ is that in the j^{th} steel layer, $\Delta\sigma^{F}$ is that in the FRP layer and $\Delta\sigma^{a}$ is that in the adhesive layer.

The out-of-plane shear stress vector τ of the concrete in the $(n+1)^{th}$ iteration due to the shear stress increment $\Delta\tau$ is

$$\left(\tau^{i+1}\right) = \left(\tau^{i}\right) + \Delta\tau^{i} \tag{38-a}$$

where

$$\Delta\tau^{i} = \left[D_{co,\mathrm{i}}\right]\left[B_{s}\right]\left\{\Delta q_{b}^{e}\right\} \tag{38-b}$$

6. Numerical Validation

Three numerical examples of FRP-strengthened RC slabs are computed to validate the proposed element CPEP. Before conducting the FE analysis, convergence studies are carried

out to study the convergence of element CPEP with the mesh refinement and the variation of the concrete layers.

6.1 Finite element analysis of a CFRP-strengthened RC slab tested by Agbossou et al. [24]

A 1250 mm × 1250 mm × 100 mm RC slab strengthened with CFRP (Slab 1) tested by Agbossou et al. [24] is analysed in this example. One layer of full-length CFRP strips, each 1 mm thick and 50 mm wide, were spaced 150 mm and bonded in the x and y directions. The bottom steel reinforcements were made of ST65C-welded square mesh ($A_s = 63.6\,\text{mm}^2$) and the top ones were made of ST35C-welded square mesh ($A_s = 38.5\,\text{mm}^2$). The tensile strength of the concrete was 2.5 MPa and its compressive strength 35.4 MPa. The Poisson's ratio of the concrete and steel was 0.2 and 0.3, respectively, the elastic modulus of the concrete, steel, FRP and adhesive was 30 GPa, 200 GPa, 80 GPa and 3.18 GPa respectively, and the tensile strength of the steel, CFRP and adhesive was 500 MPa, 925 MPa and 72.4 MPa respectively. It should be noted that, as the material properties of the adhesive were not given in Agbossou et al.'s test [24], the data was obtained from the literature [25]. The slab was simply supported on four edges with a concentrated load applied locally to its centre. Details of the FRP-strengthened RC slab are shown in Fig. 5.

A convergence test is conducted and, due to symmetry, only one-quarter of the slab is modelled. The maximum central displacement obtained from the proposed model using a 4×4, 5×5, 6×6, 7×7 element mesh with eight concrete layers and the experimental result of Agbossou et al. [24] are compared in Table 1. It can be seen that converged results can be obtained with the refinement of the mesh.

In order to study the effect of the number of concrete layers on the computed results for the element, Slab 1 is analysed using a 7×7 mesh with different numbers of concrete layers (4, 6, 8, 10 and 20). The computed maximum central displacement of the slab are presented in

Table 2 and it can be seen that the results became stable when the number of concrete layers reached 8, and the discrepancies between the computed central displacements using 6, 8 and 10 layers from that using 20 layers were all under 1%. In the following computation, for computational efficiency, one-quarter of the slab is modelled using a 7×7 mesh with the composite cross-section consisting of 8 layers of concrete, two layers of steel reinforcement, one layer of CFRP and one adhesive layer.

The load-central deflection relationship of Slab 1 obtained from the proposed model, the experimental study [24] and numerical result from Agbossou et al.'s study [24] are compared in Fig. 6 in which it can be seen that the results obtained from the current model show better agreement with the experimental than the other numerical model. The load-deflection curve from the current model and experimental study show very similar trends during the loading period with the ultimate maximum central deflection of 6.392 mm and 6.68 mm respectively.

It should be mentioned that Agbossou et al. [24] modelled the slab using ANSYS and different types of elements were used to model the concrete, steel reinforcement and FRP strips. Solid65 elements with 8 nodes and three DOFs at each node were used to model the concrete, Link8 elements with 2 nodes and three DOFs at each node were used to model the steel reinforcement and Shell99 elements with 8 nodes and six DOFs at each node were used to model the FRP strips. In total, 6296 elements (5408 Solid65 elements, 728 Link8 elements and 160 shell elements), 6561 nodes and 19,368 DOFs were used to model the slab, while only 49 CPEP elements with 64 nodes and 384 DOFs are used in the current FE model, which is much more computationally effective.

6.2 Finite element analysis of a CFRP-strengthened two-way RC slab tested by Foret and Limam [3]

A 1650 mm × 1150 mm × 70 mm two-way RC slab (Slab 2) tested by Foret and Limam [3] is analysed for further validation of the proposed plate element. The internal steel grid

reinforcements consisted of 6 mm diameter steel bars spaced 300 mm apart in the x and y directions, and the CFRP laminate was 50 mm wide and 1.4 mm thick. The tension face of Slab 2 was strengthened by CFRP strips 1000 mm wide and 1500 mm long spaced 150 mm apart in the *x* and *y* directions, respectively. The average 28-day modulus of elasticity of the concrete was 25 GPa and the elastic modulus of the steel reinforcement, CFRP and adhesive was 200 GPa, 163G Pa and 3.18 GPa respectively. The tensile strength of the steel, CFRP and adhesive was approximately 540 MPa, 2800 MPa and 72.4 MPa respectively. The slab was simply supported on four sides and subjected to a central load, and a physical model of it is shown in Fig. 7. Due to symmetry, in the current FE model, only one-quarter of the slab is analysed using a 6 × 6 mesh, with the cross-section of the concrete divided into eight layers.

The relationships between the load and central displacement obtained from the current model and experimental study [3] are compared in Fig. 8. Although there is some difference between the load-deflection curves from current model and experimental results during the initial loading stage, these curves match well after around 60 kN with computed maximum deflection of 10.31 mm using the present model and 10.766 mm from experimental results.

6.3 Finite element analysis of a CFRP-strengthened RC slab tested by Limam et al. (2003) [2]

A 1700 mm × 1300 mm × 70 mm FRP-strengthened RC slab (Slab 3) tested by Limam et al. [2] was computed using the developed model. The internal steel grid reinforcement was provided by 6 mm diameter bars spaced 200 mm apart in the x and y directions, and the concrete cover was 17 mm. 1.4 mm thick, 50 mm wide and 1500 mm long CFRP strips were bonded to the soffit of the slab in the y direction and CFRP strips with the same cross-sectional dimensions but 1000 mm long were bonded to the tension face of the slab in the x direction, all of which were spaced 150 mm apart. The average 28-day concrete compressive strength was 30 MPa and its modulus of elasticity was 25 GPa. The steel tensile yield stress strength was 540 MPa and its modulus of elasticity was 200 GPa. The tensile strength of the

CFRP and adhesive was 2800 MPa and 72.4 MPa, respectively, their moduli of elasticity was 160 GPa and 3.18 GPa, respectively. The slab was simply supported on four sides and subjected to a central load, and a physical model of it is shown in Fig. 9 Due to symmetry, only one-quarter of the slab was analysed using a 5×5 mesh with the cross-section of the concrete divided into eight layers.

Fig. 10 shows a comparison of the load versus central deflection relationship obtained from the present model and experimental study [2] in which it can be seen that the computed and experimental results agree very well until approximately 100 kN and slight difference between them is observed in the final loading stage. The computed ultimate displacement is 26.01 mm while that of from experiment is 28.09 mm.

7. Parametric Studies of Structural Behaviour of FRP-strengthened RC Slabs

Once the finite element model has been validated, parametric studies can be conducted to further investigate the structural behaviour of the structure which will provide useful reference to engineers. The effects of different parameters, such as the type of FRPs, width and thickness of FRPs on the structural behaviour of FRP-strengthened RC slabs are analysed using the present model.

Slab 3 as computed in Section 6 is used as the basic physical model for the parametric studies. The load-central deflection relationship of the slab with different parameters are presented and compared.

7.1 Effect of types of FRPs on the structural behaviour

Material properties of FRPs vary with different types. CFRP has good rigidity but relatively expensive compared to GFRP and BFRP. The strength properties of GFRP are somewhat lower than those of carbon fibres and it is less stiff, and its raw materials are much less expensive. BFRP has a similar chemical composition to GFRP but better strength

characteristics. In order to investigate the effect of the type of FRPs on the structural behaviour of the FRP-strengthened RC slab, three RC slabs strengthened with CFRP, GFRP and BFRP (denoted as Slab 3-C, Slab 3-G and Slab 3-B) are analysed using the new element. The material properties of each FRP are given in Table 3 and their configurations for strengthening are the same, with the FRP strips 1.4 mm thick and 50 mm wide.

The effect of the different types of FRPs on the structural behaviour of the RC slabs is shown in Fig. 11. It can be seen that the RC slab strengthened with CFRP exhibited stiffer behaviour after approximately 60 kN, which may be attributed to the higher elastic modulus of CFRP, while those strengthened with BFRP and GFRP, which had similar material properties, performed similarly. At a load level of about 120 kN, the central deflection with CFRP, GFRP and BFRP is 26.01 mm, 29.2 and 28.64 mm, respectively, that is, that of GFRP and BFRP is respectively, 12.26% and 10.11% greater than that of CFRP.

7.2 Effect of width of FRPs on the structural behaviour

Three RC slabs, denoted as Slab 3, Slab 3-W1, and Slab 3-W2, strengthened with 50 mm, 100 mm and 150 mm wide CFRP strips respectively are analysed to study the effect of width of the FRP on their structural behaviour. The CFRP strip is 1.4 mm thick with 150 mm spacing. The tensile strength and elastic modulus of CFRP is 2000 MPa and 160 GPa respectively.

Fig. 12 shows the computed load-central deflection relationship of the three slabs. It can be seen that the load-deflection relationships of the three slabs are generally very close and this shows that the width of strengthening FRP sheets has no significant effect on the load-deflection behaviour of the RC slabs. The curve for Slab 3-W1 and Slab 3-W2, strengthened with 100 mm and 150 mm wide CFRP strips respectively are nearly the same. The curve for Slab 3 strengthened with 50 mm wide CFRP strips is nearly the same as the other two until

the load is approximately 50 kN, where a little discrepancy appears and the discrepancy increases with the increase of applied load but the curve still agree reasonably well with other two. The Slab 3 strengthened with 50 mm wide CFRP strips has the maximum deflection which is 26.01 mm when the load is around 120 kN, while Slab 3-W1 and Slab 3-W2 produce less deflection of 25.18 mm and 24.65 mm respectively.

7.3 Effect of thickness of FRP on the structural behaviour

The commonly used thicknesses of FRP plates are 1 mm and 1.4 mm while, in engineering practice, different layers of FRP can be applied to attain the required thickness. In this study, reinforced concrete slabs strengthened with 1 mm, 1.4 mm and 2 mm (2×1 mm layers) thick CFRP plates (named Slab 3-T1, Slab 3 and Slab 3-T2) are analysed using the proposed element to investigate the effect of thickness of FRP on the structural behaviour of the slab. The computed load-central deflection of the three slabs obtained from the proposed element is compared in Fig. 13. The material properties of the CFRP are given in Table 2 and their configurations for strengthening are the same, with the FRP strips 1.4 mm thick and 50 mm wide.

It can be found from Fig. 13 that the load-deflection curves of the three slabs are very close, especially before the load reaching 50 kN. After the load of 50 kN, small discrepancy is observed from the three curves with the deflection of Slab 3-T1 of 26.34 mm which is slight (4.73%) larger than that of Slab 3-T2. The Slab 3 strengthened with 1.4 mm thick FRP plates produces nearly the same deflection as Slab 3-T2 strengthened with 2 mm thick FRP plates. Thus it can be seen that the thickness of the FRP sheets has with little effect on the flexural behaviour of the FRP strengthened RC slabs.

8. Summary

A simple 4-node 24-DOF rectangular composite layered element is developed for nonlinear FE analysis of FRP-strengthened RC slabs in this paper.

The element is a unified element with all layers modelled in one single element. The shear locking problem naturally is avoided by using Timoshenko's composite beam functions. Numerical examples demonstrated its accuracy and efficiency in predicting the structural behaviour of FRP-strengthened RC slabs. The effects of different types, widths and thicknesses of FRPs on the flexural response of FRP-strengthened RC slabs are also studied using the new element. Based on the parametric studies, the main findings are concluded.

1. Types of FRPs have significant influence on the structural behaviour of FRP-strengthened RC slabs. The CFRP-strengthened RC slab performs best comparing to the GFRP and BFRP-strengthened slabs. The central deflection of the CFRP-strengthened RC slab is the least which is 12.26% and 10.11% less than that of the slab strengthened with GFRP and BFRP. The central deflection of the RC slab strengthened with GFRP and BFRP is close which might be attributed to their similar elastic modulus.
2. The load resistance capability of FRP-strengthened RC slabs is improved with the increase of the width of the FRP strips. The RC slab strengthened with 200 mm wide FRP strips produces the least deflection compared to the one strengthened with 50 mm and 100 mm wide strips.
3. The flexural responses of FRP-strengthened RC slabs are slightly affected by the thickness of the FRP strips. The deflection of the RC slab strengthened with 2 mm and 1.4 mm thick FRP strips is about 5% less than that of the RC slab strengthened with 1 mm thick FRP strips.

References

[1] Reitman MA, Yankelevsky DZ. A new simplified model for nonlinear RC slabs analysis. ACI Structural Journal 1997;94(4):399-408.

[2] Limam O, Foret G, Ehrlacher A. RC two-way slabs strengthened with CFRP strips: experimental study and a limit analysis approach. Composite Structures 2003;60(4):467-471.

[3] Foret G, Limam O. Experimental and numerical analysis of RC two-way slabs strengthened with NSM CFRP rods. Construction and Building Materials 2008;22(10):2025-2030.

[4] Tedesco JW, Stallings JM, El-Mihilmy M. Finite element method analysis of a concrete bridge repaired with fiber reinforced plastic laminates. Computers and Structures 1999;72:379-407.

[5] Ebead UA, Marzouk H. Tension-stiffening model for FRP-strengthened RC concrete two-way slabs. Materials and Structures 2005;38(276):193-200.

[6] Oehlers DJ. Development of design rules for retrofitting by adhesive bonding or bolting either FRP or steel plates to RC beams or slabs in bridges and buildings. Composites - Part A: Applied Science and Manufacturing 2001;32:1345-1355.

[7] Meshgin P, Choi KK, Taha MMR. Experimental and analytical investigations of creep of epoxy adhesive at the concrete-FRP interfaces. International Journal of Adhesion and Adhesives 2009;29:56-66.

[8] Elsayed W, Ebead UA, Neale KW. Interfacial behavior and debonding failures in FRP-Strengthened concrete slabs. Journal of Composites for Construction 2007;11(6):619-628.

[9] Lu XZ, Teng JG, Ye LP, Jiang JJ. Bond–slip models for FRP sheets/plates bonded to concrete. Engineering Structures 2005;27:920–937.

[10] Zhang YX, Bradford MA, Gilbert RI. A layered shear-flexural plate/shell element using Timoshenko beam functions for nonlinear analysis of reinforced concrete plates. Finite Elements in Analysis and Design 2007;43(11-12):888-900.

[11] Zhang YX, Kim KS. Two simple and efficient displacement-based quadrilateral elements for the analysis of composite laminated plates. Int. J. Num. Meth. Engng. 2004; 61:1771-1796.

[12] Zhang YX, Kim KS. Geometrically nonlinear analysis of laminated composite plates by two new displacement-based quadrilateral plate elements, Composite Structures 2006;72(3): 301-310.

[13] Zhang YX, Bradford MA. Nonlinear analysis of moderately thick reinforced concrete slabs at elevated temperatures using a rectangular layered plate element with Timoshenko beam functions, Engineering Structures 2007;29:2751-2761.

[14] Zhang YX, Zhu Y. A new shear-flexible FRP-reinforced concrete slab element. Composite Structures 2010; 92(3):730-735.

[15] Lin Xiaoshan, Zhang YX. A novel one dimensional two-node shear-flexible layered composite beam element. Finite Elements in Analysis and Design 2011;47: 676–682.

[16] Zhang YX, Lin Xiaoshan. Nonlinear finite element analysis of steel/FRP-reinforced concrete beams by using a novel beam element. Advances in Structural Engineering 2013;16(2):339-352.

[17] Lin Xiaoshan, Zhang YX. Novel composite beam element with bond-slip for nonlinear finite element analyses of steel/FRP-reinforced concrete beams. Technical notes, Journal of Structural Engineering 2013;139(12):06013003-1-06013003-6.

[18] MacNeal RH, Harder RL. A refined four-noded membrane element with rotational degrees of freedom. Computers & Structures 1988;28:75-84.

[19] British Steel Construction Institute Steel Design Guide to BS5950: 1993;Part 1:1990, Vol. 1, Section Properties, Member Capacities, third edition.

[20] Carlos AC, Maria ML. Damage approach for the prediction of debonding failure on concrete elements strengthened with FRP. Journal of Composites for Construction 2007; 11(4):391-400.

[21] Gilbert RI. Time dependent behaviour of structural concrete slabs. Ph.D. Thesis, University of New South Wales, Sydney, Australia, 1979.

[22] Cedolin L, Deipoli S. Finite element studies of shear-critical R/C beams. Journal of the Engineering Mechanics Division 1977;ASCE (103):395–410.

[23] Izumo J, Shin H, Meakawa K, Okamura H. An analytical model for RC panels subjected to in-plane stresses. Concrete Shear in Earthquakes 1992:206-215.

[24] Agbossou A, Michel L, Lagache M, Hamelin P. Strengthening slabs using externally-bonded strip composites: analysis of concrete covers on the strengthening. Composites Part B: Engineering 2008;39(7-8):1125-1135.

[25] Quattlebaum JB, Harries KA, Petrout MF. Comparison of three flexural retrofit systems under monotonic and fatigue loads. Journal of Bridge Engineering 2005;10(6):731-740.

FIGURE CAPTIONS

Fig.1 A layered rectangular composite plate element.

Fig. 2 Stress-strain relationship of steel.

Fig. 3 Stress-strain relationship of FRP.

Fig. 4 Stress-strain relationship of concrete in tension (Izumo et al. 1992).

Fig. 5 The physical model of Slab 1 (Agbossou et al. 2008) (dimensions: mm)

Fig. 6 Load-central deflection relationship of Slab 1 (dimensions: mm)

Fig. 7 The physical model of Slab 2 (Foret and Limam 2008) (dimensions: mm)

Fig. 8 Load-central deflection relationship of Slab 2.

Fig. 9 The physical model of Slab 3 (Limam et al. 2003) (dimensions: mm)

Fig. 10 Load-central deflection relationship of Slab 3.

Fig. 11 Load-central deflection relationship of Slab 3 with different types of FRPs.

Fig. 12 Load-central deflection relationship of Slab 3 with different width of FRPs.

Fig. 13 Load-central deflection relationship of Slab 3 with different thickness of FRPs.

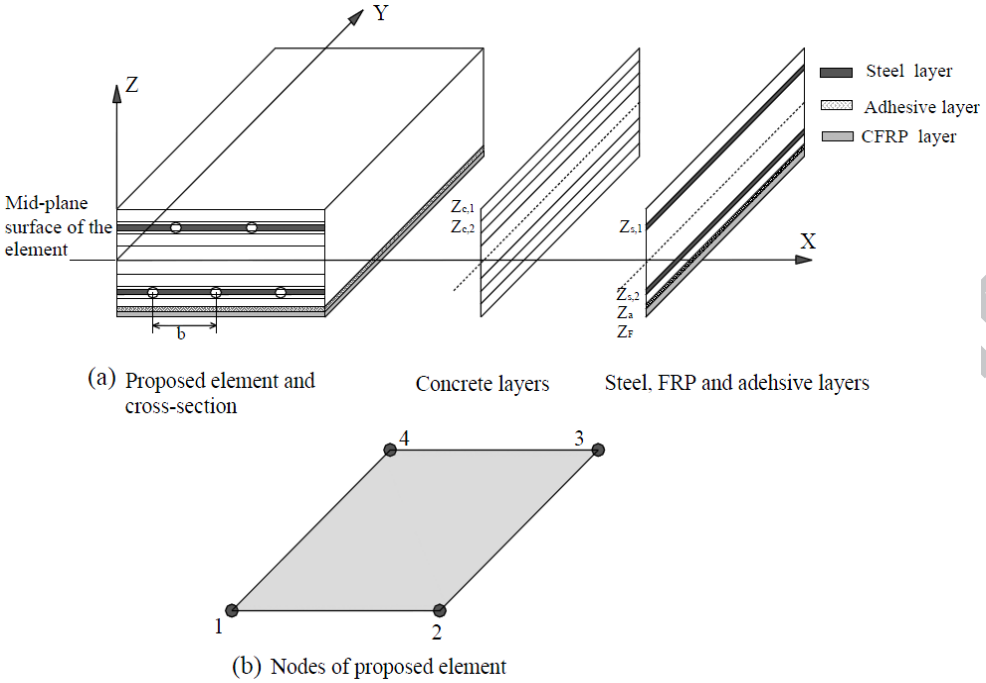

Fig. 1. A layered rectangular composite plate element

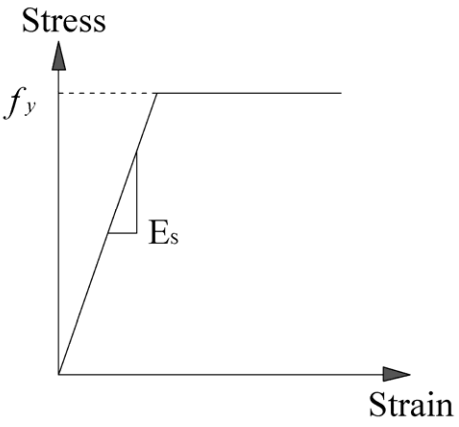

Fig. 2. Stress-strain relationship of steel

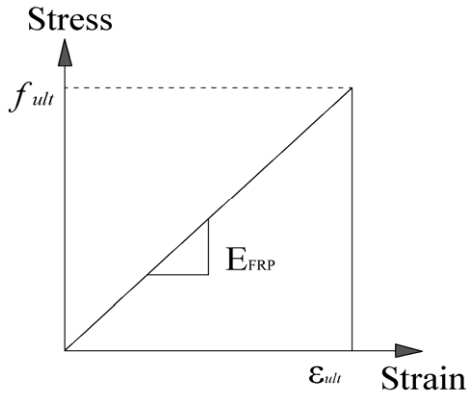

Fig. 3. Stress-strain relationship of FRP

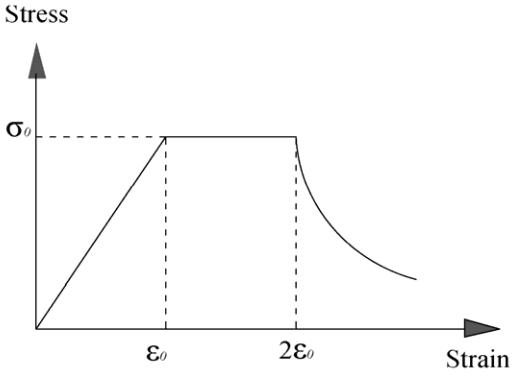

Fig. 4. Stress-strain relationship of concrete in tension (Izumo et al. 1992)

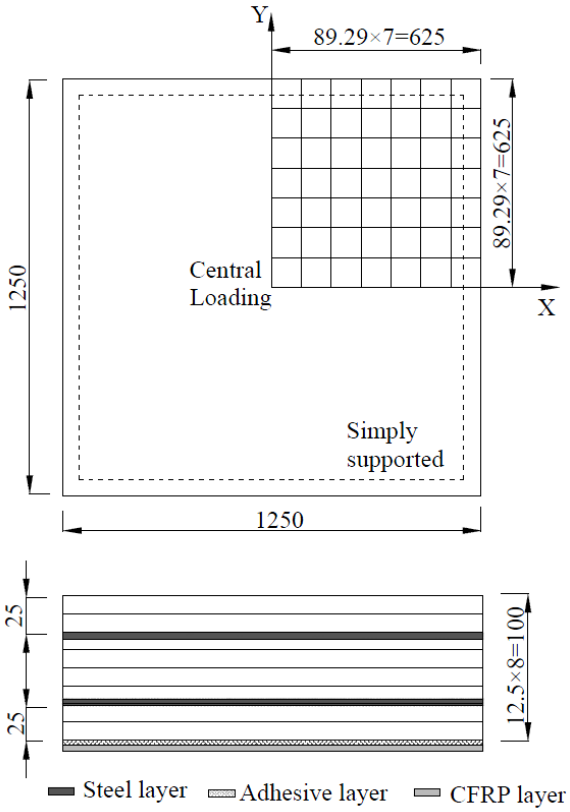

Fig. 5. The physical model of Slab 1 [24] (dimensions: mm)

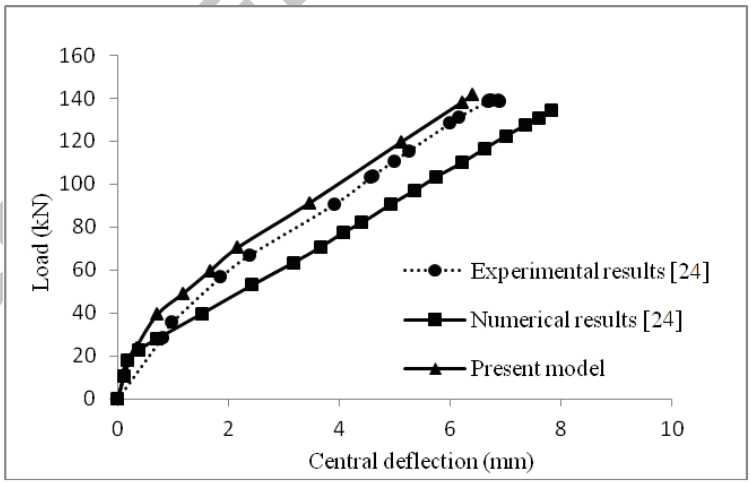

Fig. 6. Load-central deflection relationship of Slab 1 (dimensions: mm)

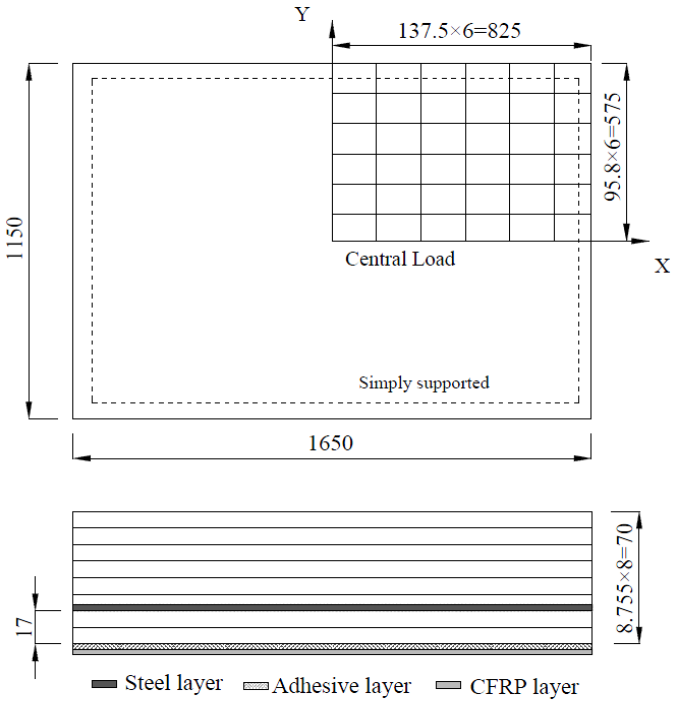

Fig. 7. The physical model of Slab 2 [3] (dimensions: mm)

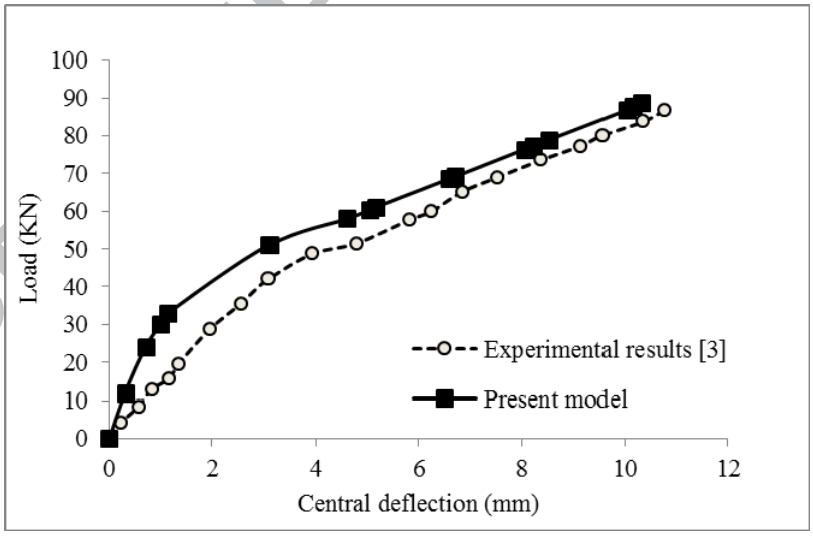

Fig. 8. Load-central deflection relationship of Slab 2

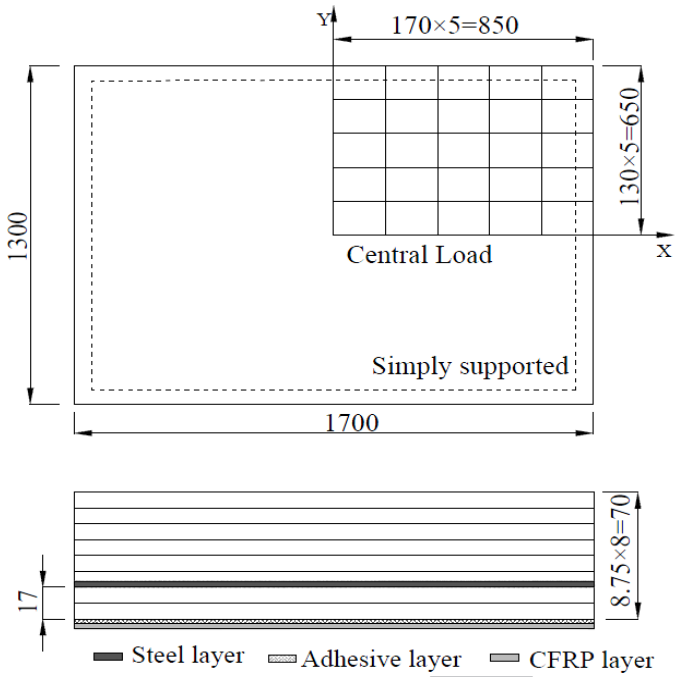

Fig. 9. The physical model of Slab 3 [2] (dimensions: mm)

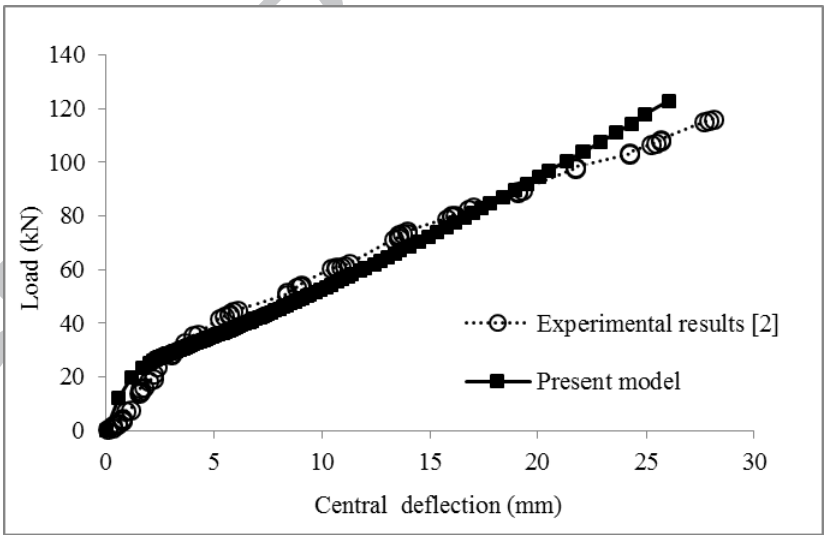

Fig. 10. Load-central deflection relationship of Slab 3

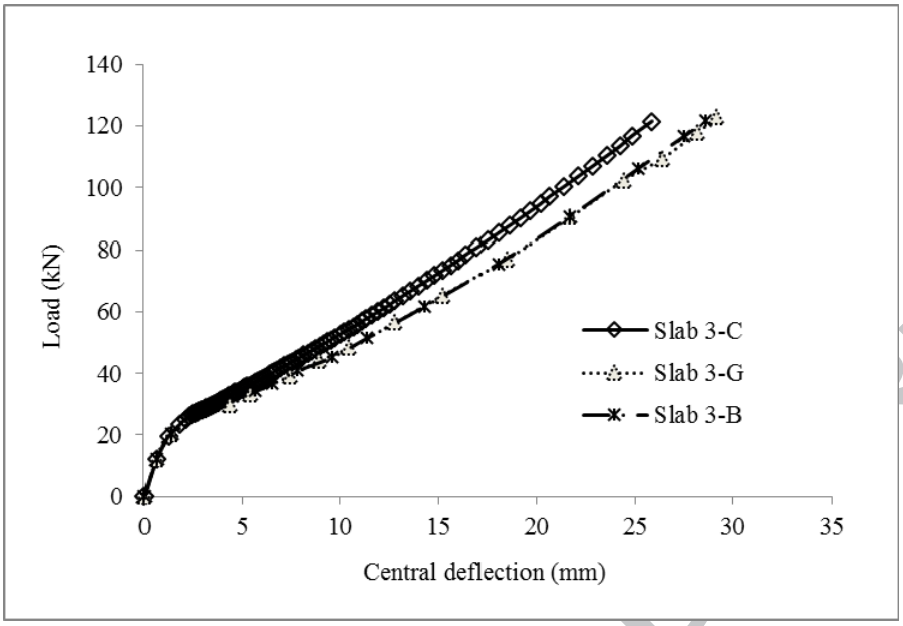

Fig. 11. Load-central deflection relationship of Slab 3 with different types of FRPs

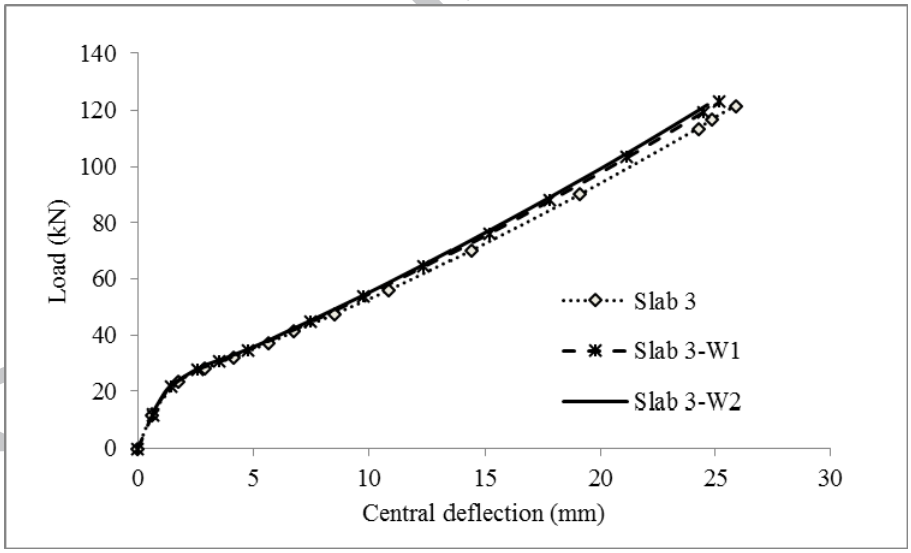

Fig. 12. Load-central deflection relationship of Slab 3 with different width of FRPs

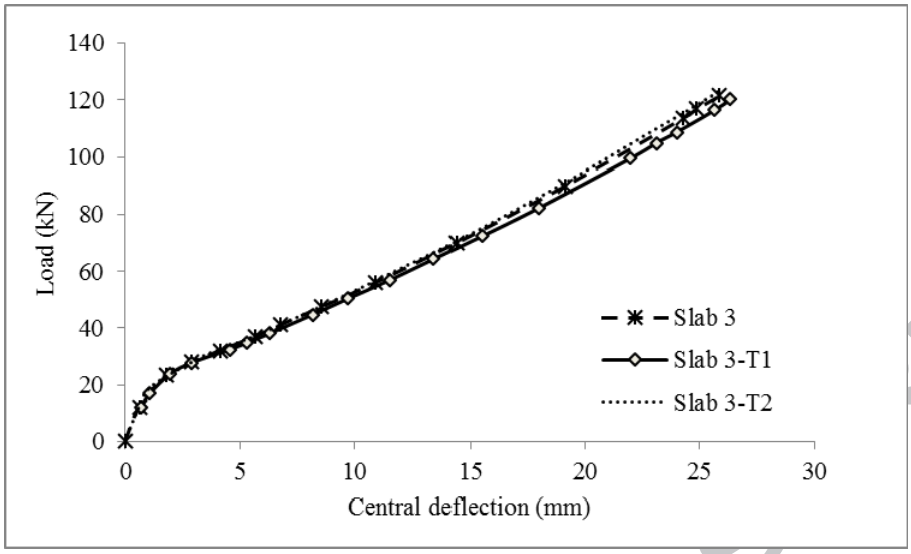

Fig. 13. Load-central deflection relationship of Slab 3 with different thickness of FRPs

TABLE CAPTIONS

Table 1 Convergence test for different number of elements for element CPEP.

Table 2 Convergence test for different concrete layers for element CPEP.

Table 3 Material properties of different types of FRPs.

Table 1

Convergence test for different number of elements for element CPEP

Number of elements	Number of nodes	The maximum displacement (mm)
4×4=16	25	6.318
5×5=25	36	6.379
6×6=36	49	6.388
7×7=49	64	6.392
Experimental result (Agbossou et al. 2008)		6.68

Table 2

Convergence test for different concrete layers for element CPEP

Number of concrete layers	The maximum deflection (mm)
4	5.85
6	6.33
8	6.392
10	6.385
20	6.379
Experimental result (Agbossou et al. 2008)	6.68

Table 3

Material properties of different types of FRPs

Material	Tensile strength (MPa)	Modulus of elasticity (GPa)
CFRP	2000	160
GFRP	1500	76
BFRP	1700	78